Simultaneous multiple surfaces method applied to infrared lenses

Thibaut Mayeur, Jean-Baptiste Volatier, Guillaume Druart, Elodie Tartas, Alain Durand, Françoise Cau

Simultaneous Multiple Surfaces method applied to infrared lenses

T. Mayeur*[a,b,c], J.B Volatier[a], G.Druart[a], E.Tartas[b], A. Durand[b], F.Cau[c]
[a]ONERA, 6 Chemin de la Vauve aux Granges, 91120 Palaiseau, France; [b]Lynred, 364 route de Valence, 38113 Veurey-Voroize, France; [c]Safran Electronics & Defense, 100 avenue de Paris, 91300 Massy, France

ABSTRACT

In optical design, the designer's experience is critical. Indeed, an experienced optical designer will often choose a better starting point for optimization than an inexperienced one. Most of the time, lens design software use a local optimization algorithm, which is why the starting point is so important to get an excellent optical system. We present here an alternative to the classical optical design method and a solution to reduce the impact of the designer's experience.

Our alternative couples the Simultaneous Multiple Surfaces (SMS) method, introduced by Benítez and Miñano with optimization in Zemax OpticStudio. The SMS method is a direct construction method of optical systems without optical aberrations for as many field points as the system contains surfaces. This method can deal with both aspheric and freeform optical systems depending on the dimension of the method implemented.

Our implementation of the SMS method can design optical systems with three surfaces. We use the SMS method to define a freeform system with an F-number of 0.85. Then, we use this fast freeform system as a starting point to perform further optimization in Zemax OpticStudio. Finally, we achieve to design two diffraction-limited freeform systems, one over a square field of view of $\pm 30°$ and another over a rectangular field of view of $\pm 33° \times \pm 26°$.

Keywords: Simultaneous Multiple Surfaces, freeform surfaces, Cartesian oval, automated method, optical design

1. INTRODUCTION

Since its inception, the design of optical imaging systems has relied on spherical surfaces and later on rotationally symmetric surfaces such as a sphere, conic, asphere, etc. However, in the 70's, the first optical system with a surface without rotational symmetry was commercialized [1]. In this article, freeform surface refers to surfaces without rotational symmetry [2]. An optical design always aims at finding an optimum between conflicting requirements. For example, in many fields of application (space, defense, automotive), optical performance and minimization of volume are both essential. By bringing more degrees of freedom to the designer, freeform systems can out-compete classical systems on all requirements. For example, literature has shown that off-axis catoptric freeform systems bring a volume reduction of 66% to a similar optical performance point [2].

However, freeform surface brings new challenges to optical design. The choice of the representation basis of surfaces (Zernike polynomials, XY polynomials, etc.) will affect the result. Moreover, the utilization of freeform optics makes the optimization of the MF more complex due to a large number of degrees of freedom. In turn, this increases the impact of the designer's experience even more than the design of classical systems, where it is common knowledge that the designer's experience affects the result already significantly. Therefore, a freeform system is often the improvement of a classical design like the Three-Mirror Anastigmat (TMA) design.

New design methods appeared in the last decade to handle and simplify this problem. We can sort them into two categories: direct construction and optimization methods. In direct construction methods of interest, we can single out the SMS method [3]–[17], the point-by-point method [18], [19], or the differential ray tracing method [20], [21]. One advantage of direct construction methods is that they avoid specifying a starting point unlike optimization methods in optical design software. Using a direct construction method also allows choosing the representation basis of surfaces later or starting the optimization with a freeform system instead of a classical one.

Regarding these new methods, the SMS method seems promising for applications such as Advanced Driver-Assistant Systems (ADAS), where infrared foveated vision systems with large apertures and fields could play an

important role [site Heliaus]. Our implementation of the method is based on the previous works of Benítez and Miñano's team [1–4], describing the principle of the method. This article will describe our understanding and implementation of the SMS method using Python and Zemax OpticStudio. We will focus on the SMS 3 surfaces in the 3D method (SMS-3S-3D).

2. PRINCIPLE OF THE SMS METHOD

2.1 Cartesian oval and its generalization

A Cartesian oval is a surface that couples an incident wavefront and an outcoming wavefront. That principle implies that an imaging Cartesian oval perfectly images one point of the object or the field. Figure 1 shows an example of a Cartesian oval. In that case, the Cartesian oval is a parabola because the surface couples a parallel on-axis wavefront to a spherical one (perfect image). To design an imaging Cartesian oval, we must set the point of the field we want to image perfectly and its ideal image through the surface. We have two possibilities to impose the image of the chosen field through the Cartesian oval: either we can set the optical path length of the rays or directly the image coordinates.

The SMS method is based on the Cartesian oval principle. It is a generalization of this principle, where the method constructs a system of N surfaces (N Cartesian ovals) with N aberration-free fields (SMS-NS). We note SMS-2S method, the SMS method that constructs a system of 2 surfaces.

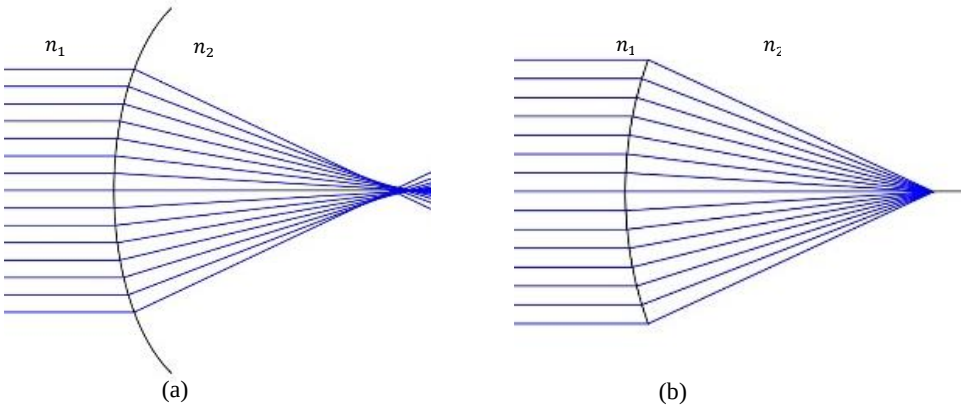

Figure 1. (a) Spherical surface, (b) Cartesian oval (it is a parabola here).

2.2 Standard flowchart of the SMS method and differences between SMS-2S and SMS-NS (N > 2)

We can make a standard flowchart of the SMS method (see Figure 2). There are differences in the implementation between SMS-2S and SMS-NS (N>2) methods. The first difference appears at the early stage of the SMS method at the initial parameters setting step. Some parameters are common to all the SMS methods, and others rely on the SMS method used:

- Common parameters:
  - Studied fields
  - F-number ($F/\#_{\text{target}}$)
  - Focal length
  - Refractive index
- SMS-2S parameters:
  - A point and its normal vector (SMS-2S-2D)
  - A curve defined by a point cloud and its normal vectors (SMS-2S-3D)
- SMS-NS parameters:
  - Some curved radii of the surfaces (two curved radii for SMS-3S)
  - Thicknesses between surfaces

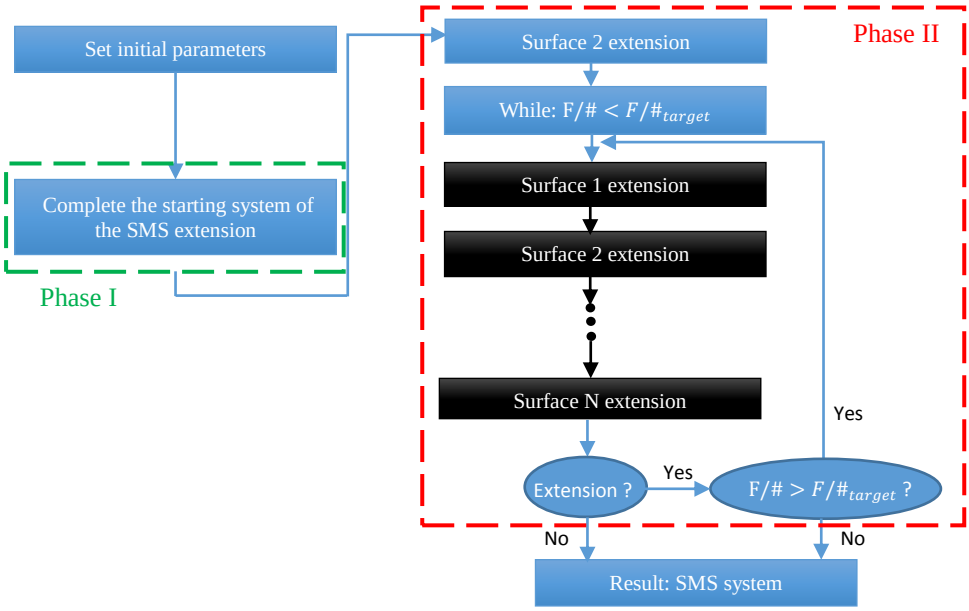

Figure 2. Standard flowchart of the SMS method.

After this difference at the initial parameters setting step, two other differences make the SMS-NS harder to apply than the SMS-2S. The first one is that the SMS-2S method does not need the "Phase I" step of the flowchart, where we compute the starting system of the SMS extension. Because the initial parameters set are sufficient to begin the SMS extension, we do not require other information on the starting system. In contrast, this step is necessary for the SMS-NS as it defines the different surfaces close to the optical axis. In reality, the discrepancy in the complexity comes from the last remaining difference, which is that SMS-2S methods do not require any interpolation or approximation of the designed surfaces during Phase II (SMS extension), while SMS-NS methods do.

In SMS-NS methods, we can clearly distinguish SMS-NS-2D and SMS-NS-3D in terms of complexity and computation time. This distinction comes from the fact that the approximation process is entirely different. For the SMS-NS-2D, we perform only a curve approximation, whereas, for the 3D method, we have to perform a surface approximation that is more complex and needs more computation time. The curve approximation used for the SMS-NS-2D is a sum of parabolic approximation for each slice of the different surfaces we construct. This approximation method has a reasonable complexity, so it does not add much computation time to the SMS-NS-2D. On the contrary, the approximation process for SMS-NS-3D, where we have to compute an approximation of surfaces that is heavy to implement and increases the computation time significantly. We have decided to implement the approximation method called "Cubic Local Patch" (CLP) described in the SMS literature [2]. This approximation method uses Non-uniform rational Basis Spline (NURBS) to approximate a point cloud. This surface representation is powerful as it can represent locally or globally any surface. Those two properties are interesting in the case of the SMS method because we want to limit the initial hypothesis over the system and describe the surfaces locally, enabling us to design more wild freeform surfaces.

Now that we have described the general principle of the SMS method and some of the implementation issues, we will explain our implementation of the SMS-3S-3D method in more detail.

3. SMS-3S-3D METHOD

3.1 Initial settings

To begin the SMS-3S-3D algorithm, we have to set the initial parameters. Using SMS-3S for refractive systems means we have to fix one surface and perfectly define it because we cannot have an odd number of surfaces. Therefore, applying the SMS-3S-3D method, we design a system of 4 surfaces with 3 SMS surfaces and one fixed surface. To be clear on what are the initial parameters to set and to declare the notations that we use in this article, we list the settings:

- Focal length: f
- Fields to correct: $\theta_0 = +\theta_{max}$, $\theta_1 = 0°$, and $\theta_2 = -\theta_{max}$ (we use Zemax's convention for the angles)
- Targeted images: $Target_0$, $Target_1$ and $Target_2$ respectively for field 0, 1 and 2
- Refractive index of the two lenses: n_1 and n_2
- F-number: $F/\#_{target}$
- Thicknesses: zs_1, zs_2, zs_3 and zs_4 positions along the Z-axis of the vertex of surfaces 1, 2, 3 and 4
- Radius of curvature: R_1, R_2, and R_4 radius of curvature respectively of surfaces 1, 2 and 4
- Fix the known surface: in our implementation, we fix surface four as the known surface (arbitrary choice)
- Set the sag equation of surface 4: $Sag_4 = \frac{cr^2}{1+\sqrt{1-(1-k)c^2r^2}} + zs_4; c = \frac{1}{R_4}$; k: conic constant (in our implementation, surface 4 is a spherical surface, but it can be any surface, it just has to be defined)

3.2 Description of Phase I

Phase I is essential for the SMS-3S-3D method performance because it completes the starting system of the SMS extension [3]. We can separate Phase I into different steps (see Figure 3). We change the step order depicted in the thesis of M. Nikolic [5] to simplify the implementation. Still, this modification does not change the operation of Phase I. We illustrate the different steps of Phase I in Figure 3, where Figure 3 (a) shows the initial settings of the system before running Phase I. To explain the other sections of the figure, we list the different steps and their principles:

1. **Computation of the central curve of surface 3 (see Figure 3 (b)).** We trace multiple rays of field θ_1 through the central curve (Y = 0) of surface 1. The targeted F-number directly defined the X-width of this curve as we consider surface 1 as the pupil of the system. Using this information, we compute the central curve of surface 2 and the refracted rays. Then to compute the central curve of surface 3, we optimize a system of equations equalizing the optical path length of the different rays. We achieve the equalization using an optical path length reference that we compute using the chief ray of field 1. After performing the optimization, we obtain multiple points of surface 3 and their normal vectors. Those points define the central curve of surface 3, noted $S3_0$.

2. **Computation of the bottom edge curve of surface 1 and the top edge curve of surface 3 (see Figure 3 (c)).** Using the computed central curve of surface 2, we calculate the bottom edge curve of surface 1. This curve refers to the points of surface 1 where the refracted rays of field 0 intersect the central curve of surface 2. As before, we optimize another system of equations based on the equalization of the optical path length. We compute the top edge curve of surface 3 and the normal vectors to this curve. We refer to this curve as $S3_1$.

3. **Computation of the bottom edge curve of surface 3 (see Figure 3 (d)).** Using the XZ plane symmetry of the problem, we compute the bottom edge curve of surface 3 (noted $S3_2$) as step 2, just using this time field 2.

4. **Approximation of surfaces 1 and 3 (see Figure 3 (e)).** After the three first steps, we have computed three curves defining surface 3 but we do not have for the moment a continuous surface that is required to start the SMS extension. To obtain a continuous surface, we must perform an approximation of the surface. We approximate surface 3 using the CLP algorithm. We perform the same approximation for surface 1 to describe surface 1 on the same surface representation than surface 3.

Running those steps, we obtain the mandatory starting system for the SMS extension (see Figure 3 (e)), then we can pass to Phase II, the SMS extension.

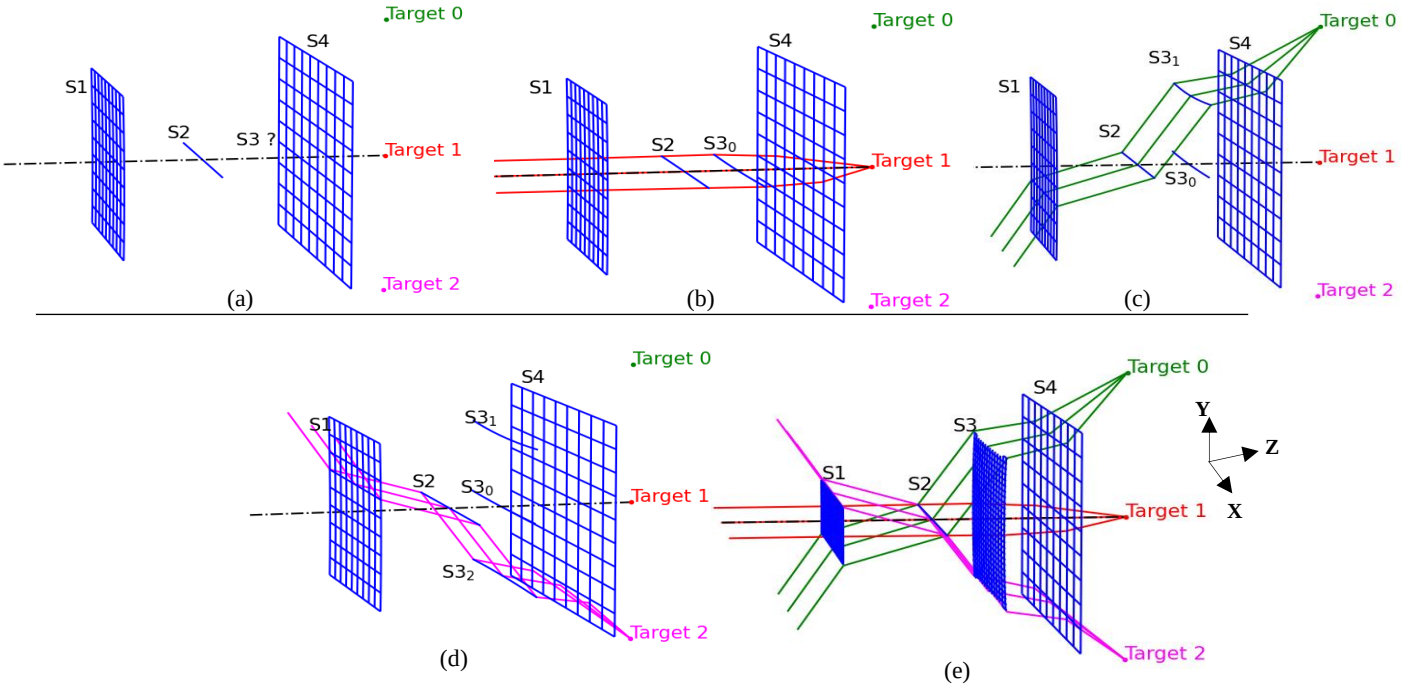

Figure 3. (a) Layout of the system before Phase I; (b) Layout of the system after the first step of Phase I; (c) Layout of the system after step 2; (d) Layout of the system after step 3; (e) Result of Phase I: layout of the starting system of the SMS extension.

We noticed that the starting system affects the SMS system's quality resulting from the SMS algorithm. To differentiate the quality of SMS systems, we look at their aperture size and not their optical quality. It is non-sense to consider their optical quality to differentiate their quality, as they are all diffraction-limited by the definition of the SMS method. Therefore, the lower the F-number is, the better is the SMS system. The optimal quality of an SMS system is reached when the F-number of the SMS system is inferior to the F-number targeted in the specifications.

3.3 Description of Phase II

This chapter will briefly describe Phase II of the SMS-3S-3D method as it is already described in the literature [5] and relies on the same principle as other SMS methods for the extension part [3], [7]. We extend the different surfaces regarding a fixed optical quality criterion. We use the description of Phase II made in the thesis of M. Nikolic [5] to implement our SMS extension, changing the optical quality criterion only. In our implementation, we based the calculus of the optical quality on the spot radius and not on the equalization of the optical path length. We chose this optical quality criterion because it is more understandable. It is easier to determine the maximum acceptable spot radius than the maximum acceptable optical path length difference. We set the maximum allowable spot radius equal to $r_{\max} = \frac{r_{\text{Airy}}}{10}$.

Before, the successive extension of the surfaces, we first have to extend surface 2 as we only have a curve to describe it. Therefore, we cannot extend another surface than surface 2 because que cannot trace rays through it at this time. To extend surface 2, we trace rays of field 1 from the image space to the object. Therefore, we trace a fan of rays from $Target_1$ to surface 3. After we must optimize a system of equations based on the chosen optical quality criterion, to compute new points of surface 2 and their normal vectors that form a point cloud (see Figure 4 (a)). Now that we have multiple points on surface 2, we can approximate the found point cloud using the CLP algorithm (see Figure 4 (b)).

Now that we have the first extension of surface 2, we can run the "While" loop described in Figure 2. The "While" loop enables the extension of the three surfaces one after the other. As a reminder, the extension of a surface consists in tracing rays of a field that pass through known parts of other surfaces and an unknown part of the surface to extend. There are two-stop conditions for the "While" loop. We list both here:

- SMS system reaches the targeted F-number
- Phase II fails in extending any surface

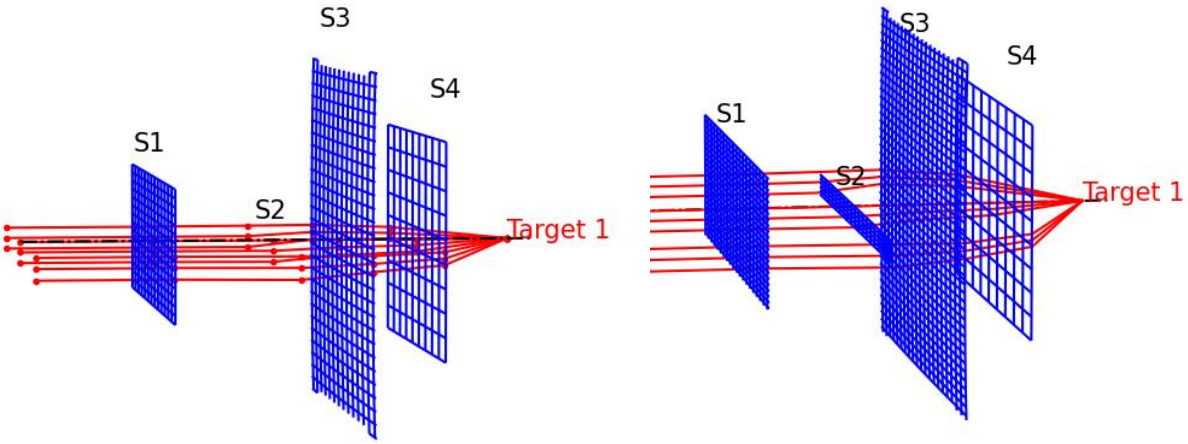

(a) (b)

Figure 4: (a) Layout of the rays allowing the extension of surface 2; (b) Layout of the system after the first extension of surface 2

The "While" loop allows the successive extension of the three surfaces. After each extension follows an approximation of the found point cloud using the CLP algorithm.

4. CASE OF STUDY OF ADAS USING THE COUPLED METHOD: SMS-3S-3D + OPTIMIZATION IN ZEMAX

4.1 Explanation of the coupled method

The coupled method uses the advantages of the SMS method in finding a starting point and optimization in optical design software. Indeed, the SMS method brings a starting system for further optimization with the excellent property of being already aspherical or freeform with few initial hypotheses on the surfaces. Starting an optimization with a freeform starting system enables the optimization to design more wild freeform surfaces than starting the optimization with a

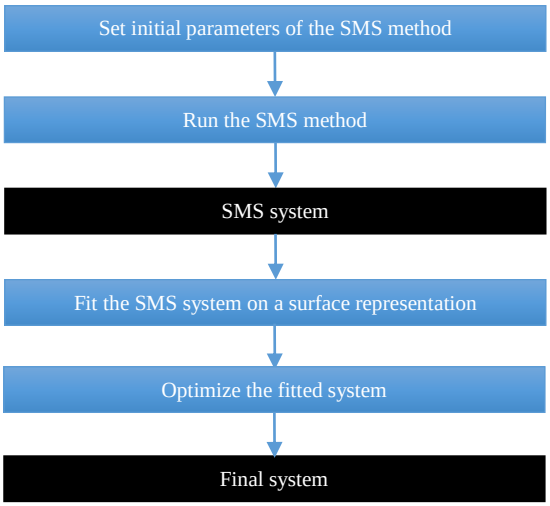

Figure 5. Flowchart of the coupled method.

rotationally symmetric system where we add some freeform terms along the optimization. The optimization part in optical design software brings the uniformization of the correction over the entire field of view (FOV). Figure 5 resumes the flowchart of the coupled method. The flowchart shows a step where we fit the SMS system on a surface representation. This fit is mandatory to perform an optimization in optical design software. We used to fit on the XY polynomial basis, but any other surface representation capable of representing a freeform surface will work.
To evaluate the capabilities of the coupled method we decided to use it to design ADAS working in the long-infrared spectrum.

4.2 Current context for ADAS

With the apparition of autonomous vehicles, the automotive industry is looking for new technologies that will answer to challenges brought by autonomous vehicles and other forms of personal mobility that change the road environment. To respond to those new needs and expectations, the European Commission identifies photonic technology as a Key Enabling Technology (KET). The automotive industry needs photonic technologies for smart mobility. Photonic technologies must be reliable, affordable, and bring versatile perception systems to handle smart mobility challenges. ADAS working in the long-infrared wavelength (LWIR) is one of the various perception systems developed to respond to smart mobility challenges. The issue with LWIR sensors is that they are expensive due to the detector price. Nevertheless, current works on reducing the pixel pitch [22], [23] allow the reduction of the detector size to decrease its price. Therefore, the price of LWIR sensors is now affordable enough to be commonly used in the automotive industry.

The reduction of the pixel pitch up to 10 µm, and recently up to 8.5 µm [23] for LWIR uncooled detectors imposes higher apertures for LWIR optical systems. The minimum F-number asked for a LWIR ADAS is now under 1.2, and the automotive industry often asks for an F-number of 1. To increase the F-number of a system while keeping the optical quality constant, optical designers usually add optical elements to the system. This working approach is unsuitable for LWIR ADAS as we want them to keep their affordability. To solve this challenge, optical designers are currently investigating freeform surfaces because they could keep the number of surfaces constant while reaching the required aperture and optical quality for ADAS.

4.3 ADAS with a square FOV

LWIR ADAS use case features found in [22], [23] inspired the current case of study. The studied ADAS must be compact, with a low F-number and a relatively large FOV. Then, the targeted system has the following features:

- Focal length: 4.8 mm
- F-number: ≤ 1.0
- Square FOV of $\pm 30°$
- The last surface is plane (surface 4)
- Working wavelength: 8-12 µm
- Material: lens number 1 (L1) in a chalcogenide glass called TGG with a refractive index of 3.39 [24] and lens number 2 (L2) in Silicon (Si) with a refractive of 3.47
- Thickness of L2: $\leq$ 1.0 mm

Regarding the features of the system that we have to design, the settings of the SMS-3S-3D method are:

- Focal length: 4.8 mm
- Refractive index: 3.39 (TGG) and 3.47 (Si)
- F-number: 0.85
- Linear FOV of $\pm 45°$ (equal to the diagonal of a $\pm 30°$ square FOV)
- The last surface is plane (surface 4)

Running the SMS-3S-3D algorithm with those initial settings, we managed to design a SMS system with an F-number equal to 0.845. The SMS algorithm took 160 seconds to be entirely performed with a standard desktop laptop (8 Go of memory and an Intel Core i5-8365U processor). The computation time can be significant due to the significant number of points necessary to calculate to well-define the surfaces and perform a good approximation of the surfaces during the algorithm. Finally, we fit the SMS system on the XY-polynomial basis to optimize the system further and

equalize the correction over the square FOV. Based on the problem's symmetry, we fit the surfaces only on symmetrical terms, but we do not impose that X and Y terms are equals. Otherwise, we would come back to rotationally symmetric surfaces. We fit up to the 8th degree of the XY polynomial basis, so we perform the fit on fourteen terms for each surface. The typical root-mean-square error of the fit is inferior to 1 µm, leading to an acceptable degradation of the correction for the four design fields, but this degradation remains acceptable. Fit error is greater at the edges than at the center of the surface. The sampling of the surface causes this. In fact, we compute more points at the center than at the edges of a surface. Consequently, rays passing through the edges of surfaces will be more aberrant than the rays passing through the center of the system.

4.4 Analysis of both systems: the fitted SMS system and the optimized system

We begin with the analysis of the fitted SMS system. Figure 6 shows the spot diagram of the three fields for the fitted system. We observe that the RMS spot radiuses of the two extreme fields are significant (200 µm). In reality, it is not important that we have huge RMS spot radiuses, as we will perform optimization with Zemax Optics Studio software. In fact, after the first optimization on the spot radius criterion using only the polynomial coefficients as variables, we successfully erased those errors due to the fit of the SMS system.

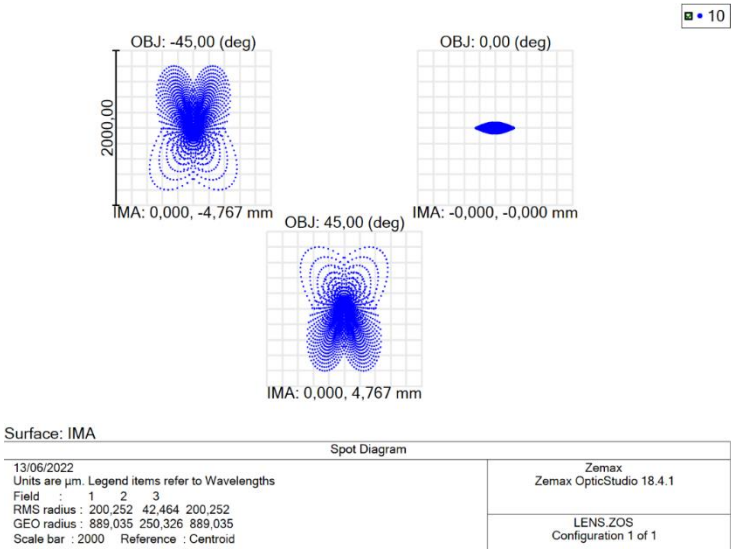

Figure 6: Spot diagram of the system fitted on the XY polynomial basis

Following the first optimization, we perform another optimization adding all thicknesses as variables and using the wavefront criterion proposed in the Zemax optimizer. During the optimization, we set constraints over thicknesses to get a final system as compact as possible and with the constraint over the thickness of L2. We obtain the optimized system shown in Figure 7 (a). The system is diffraction-limited over the entire FOV, as shown by the system's RMS spot radius field map (see Figure 7 (b)). The maximum RMS spot radius is 10.4 µm, while the airy radius is 10.44 µm.

The system obtained by applying the coupled method has the followings specifications:

- Focal length: 4.84 mm
- Entrance pupil diameter: 5.64 mm
- F-number: 0.864
- Square FOV: 31.82°
- Maximum RMS spot radius: 13.7 µm
- L1 in TGG and L2 in Si with a central thickness of 1 mm
- Total axial track: 16.6 mm

The designed system respects the specifications while succeeding to be diffraction-limited except for the four corner fields where it is very close to it. We now look at the different shapes of the surfaces. Figure 8 shows the shapes of the 3 surfaces where we removed the best-fit sphere. We observe that surface 1 and surface 3 are rotationally symmetric

surfaces. Surface 2 remains a little freeform but is very close to having rotational symmetry. We would have predicted this, considering that we optimize the freeform starting system for a rotationally symmetric problem.

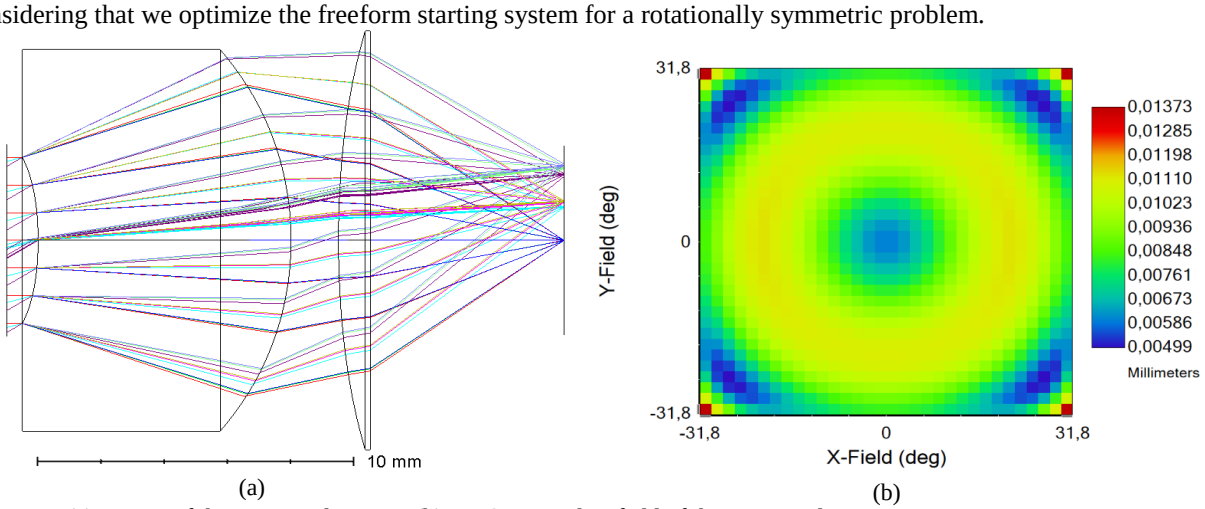

(a) (b)

Figure 7. (a) Layout of the optimized system; (b) RMS spot radius field of the optimized system

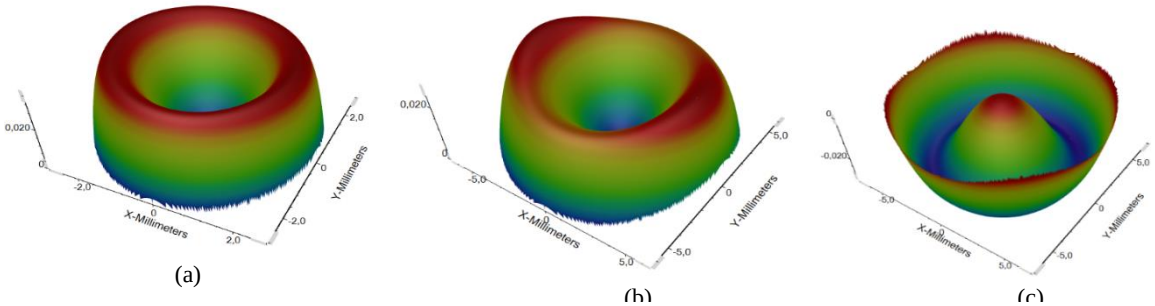

(a) (b) (c)

Figure 8: Shapes of the surfaces removing the best fit sphere. (a) Sag of surface 1; (b) Sag of surface 2; (c) Sag of surface 3

4.5 ADAS adapting the FOV to the detector's features

This study aims to adapt the FOV to the detector's size, doing that, we optimize the system only on the useful FOV [26], [27]. This optimization will lead to freeform surfaces as we optimize the system for a problem breaking the rotational symmetry (rectangular FOV). For our study, we work with a VGA detector of 640×480 pixels with a pixel pitch of 10 µm [22]. Taking into account the size of the detector and the focal length of 4.8 mm, we obtain a rectangular FOV of $\pm 33.7° \times \pm 26.6°$. This rectangular FOV is close to the system depicted in section 4.3. Therefore, we decided to use the same starting point we obtained using the SMS-3S-3D method. Nevertheless, this time the problem breaks the rotational symmetry, so using a freeform starting system for the optimization is helpful because the best final system will be a freeform system. Running the same optimization process as in section 4.3, we reach the freeform system below (see Figure 9).

The features of the freeform system are:

- Focal length: 4.86 mm
- Entrance pupil diameter: 5.64 mm
- F-number: 0.866
- Rectangular FOV: $\pm 33.7° \times \pm 26.6°$
- Maximum RMS spot radius: 11.1 µm
- L1 in TGG and L2 in Si with a central thickness of 1 mm
- Total axial track: 16.9 mm

The system is diffraction-limited for its FOV (see Figure 9 (b)), and its correction is better than the standard system optimized on the square FOV. To verify this, we compute the mean RMS spot radius of both systems, and we obtain that the freeform system has a mean RMS spot radius of 8.42 µm, while for the standard system is equal to 9.14 µm. Then,

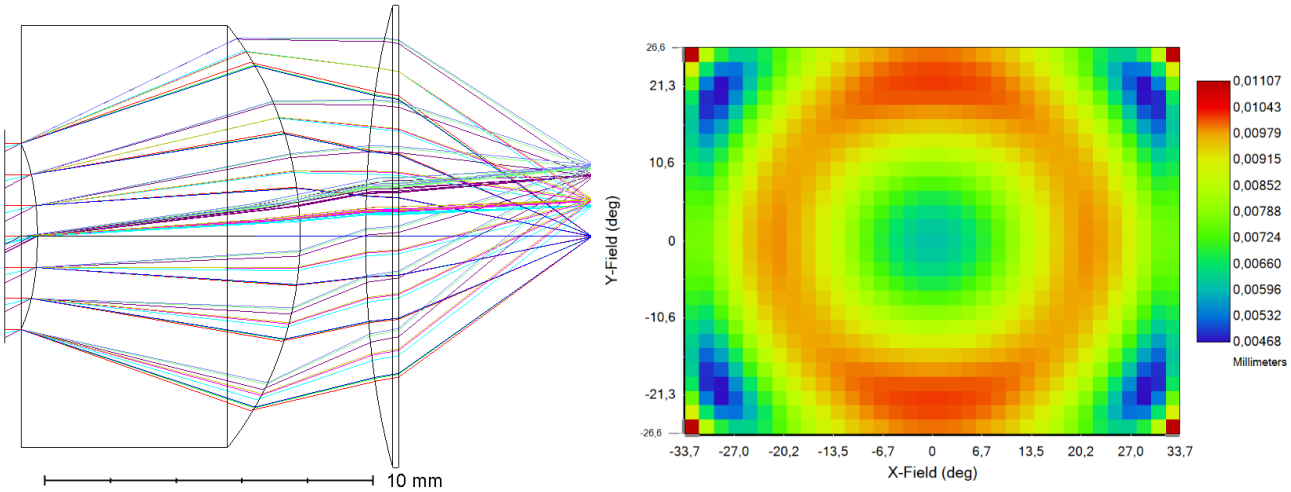

Figure 9: Results of the system optimized on a rectangular FOV. (a) Layout of the system; (b) RMS spot radius field map

adapting the FOV to the detector's size leads to a system that has a better optical quality since it focused its correction on the useful fields.

Looking at Figure 10, we see that we design a freeform system. We can notice that the first surface is nearly rotationally symmetric, but the two remaining surfaces are freeform surfaces with two planes of symmetry (XZ and YZ).

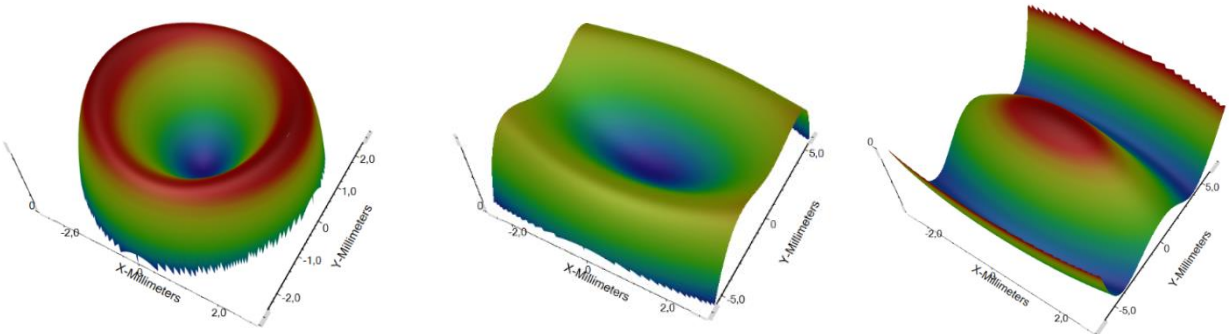

(a) (b) (c)

Figure 10: Shapes of the surfaces removing the best fit sphere. (a) Sag of surface 1; (b) Sag of surface 2; (c) Sag of surface 3

5. CONCLUSION

We have shown our implementation of the SMS-3S-3D and justified the different modifications we made compared to the implementation depicted in the literature. We use the SMS-3S-3D method as a freeform starting system generator for further optimization in optical design software.

This article shows two optical designs for ADAS application obtained using first the SMS-3D-3S and then an optimization in Zemax. First, we showed a nearly rotationally symmetric system that is diffraction-limited for a FOV of $\pm 31.8°$ and with a F-number of 0.86. After, we demonstrated the possibility of using this method to solve a non-rotational symmetric problem, where the FOV considers the detector's size. Using this methodology, we succeed in

designing such a system. The designed freeform system is diffraction-limited over a FOV of $\pm 33.7° \times \pm 26.6°$ with a fast F-number of 0.86.

This coupled method (SMS + optimization in optical software) aims to be automated to reduce the impact of optical designers' experience on the optical quality of the system. This method can also be an alternative to the classical design method for freeform. It limits the wildness of freeform surfaces by starting the optimization with a rotationally symmetric system. Conversely, the coupled method allows starting with a system that can be already freeform depending on the choice of the polynomial basis used to fit the SMS system. So in the future, we aim at applying this method to design system solving non-rotational symmetric problem.

ACKNOWLEDGEMENT

The authors would like to acknowledge the National Technology Research Association (ANRT), Safran Electronics & Defense, Lynred and ONERA for funding this research program.

DISCLAIMER

REFERENCES

[1] W. T. Plummer, 'Unusual optics of the Polaroid SX-70 Land camera', *Appl. Opt.*, vol. 21, no. 2, p. 196, Jan. 1982, doi: 10.1364/AO.21.000196.

[2] J. P. Rolland *et al.*, 'Freeform optics for imaging', *Optica*, vol. 8, no. 2, p. 161, Feb. 2021, doi: 10.1364/OPTICA.413762.

[3] P. Benitez, 'Simultaneous multiple surface optical design method in three dimensions', *Opt. Eng.*, vol. 43, no. 7, p. 1489, Jul. 2004, doi: 10.1117/1.1752918.

[4] L. Wang, 'Advances in the Simultaneous Multiple Surface optical design method for imaging and non-imaging applications', Thesis, 2012.

[5] M. Nikolić, 'SMS for imaging systems using free-forms', PhD Thesis, Universidad Politécnica de Madrid, 2017. doi: 10.20868/UPM.thesis.46748.

[6] R. Mohedano *et al.*, 'Notes on the design of free-form optics', in *AI and Optical Data Sciences*, San Francisco, United States, Feb. 2020, p. 3. doi: 10.1117/12.2547832.

[7] J. C. Miñano, P. Benítez, W. Lin, F. Muñoz, J. Infante, and A. Santamaría, 'Overview of the SMS design method applied to imaging optics', San Diego, CA, Aug. 2009, p. 74290C. doi: 10.1117/12.827068.

[8] W. Lin, P. Benítez, J. C. Miñano, J. Infante, and G. Biot, 'Progress in the SMS design method for imaging optics', San Diego, California, USA, Sep. 2011, p. 81280F. doi: 10.1117/12.894420.

[9] F. Muñoz *et al.*, 'Novel fast catadioptric objective with wide field of view', San Diego, California, Aug. 2010, p. 77800T. doi: 10.1117/12.862156.

[10] J. C. Miñano and J. C. González, 'New method of design of nonimaging concentrators', *Appl. Opt.*, vol. 31, no. 16, p. 3051, Jun. 1992, doi: 10.1364/AO.31.003051.

[11] J. C. Miñano, P. Benítez, W. Lin, J. Infante, F. Muñoz, and A. Santamaría, 'An application of the SMS method for imaging designs', *Opt. Express*, vol. 17, no. 26, p. 24036, Dec. 2009, doi: 10.1364/OE.17.024036.

[12] L. Wang, P. Benítez, J. C. Miñano, J. Infante, M. de la Fuente, and G. Biot, 'Ultracompact SWIR telephoto lens design with SMS method', San Diego, California, USA, Sep. 2011, p. 81290I. doi: 10.1117/12.894417.

[13] F. Corrente, P. Benítez, W. Lin, J. C. Miñano, and F. Muñoz, 'SMS design and aberrations theory', Barcelona, Spain, Dec. 2012, p. 855010. doi: 10.1117/12.981163.

[14] J. Liu, J. C. Miñano, P. Benítez, and L. Wang, 'Single optical surface imaging designs with unconstrained object to image mapping', Barcelona, Spain, Dec. 2012, p. 855011. doi: 10.1117/12.981210.

[15] J. Mendes-Lopes, P. Benítez, and J. C. Miñano, 'Design of diffractive optical surfaces within the SMS design method', *Imaging Appl. Opt.*, p. 3, 2015.

[16] P. BenItez, R. Mohedano, and J. C. Miñano, 'Design in 3D geometry with the Simultaneous Multiple Surface design method of Nonimaging Optics', p. 11.

[17] O. Dross *et al.*, ‘Review of SMS design methods and real-world applications’, Denver, CO, Sep. 2004, p. 35. doi: 10.1117/12.561336.
[18] T. Yang, J. Zhu, X. Wu, and G. Jin, ‘Direct design of freeform surfaces and freeform imaging systems with a point-by-point three- dimensional construction-iteration method’, p. 14, 2015.
[19] T. Yang, J. Zhu, W. Hou, and G. Jin, ‘Design method of freeform off-axis reflective imaging systems with a direct construction process’, p. 13, 2014.
[20] J.-B. Volatier and G. Druart, ‘Differential method for freeform optics applied to two-mirror off-axis telescope design’, *Opt. Lett.*, vol. 44, no. 5, p. 1174, Mar. 2019, doi: 10.1364/OL.44.001174.
[21] J.-B. Volatier, Á. Menduiña-Fernández, and M. Erhard, ‘Generalization of differential ray tracing by automatic differentiation of computational graphs’, *J. Opt. Soc. Am. A*, vol. 34, no. 7, p. 1146, Jul. 2017, doi: 10.1364/JOSAA.34.001146.
[22] G. Druart *et al.*, ‘Evaluation of the potential of high index chalcogenide lenses for automotive applications’, in *Advanced Optics for Imaging Applications: UV through LWIR VII*, Orlando, United States, May 2022, p. 16. doi: 10.1117/12.2618287.
[23] G. Druart *et al.*, ‘Study of an infrared hybrid chalcogenide silicon lenses compatible with wafer-level manufacturing process for automotive applications’, in *Optical Design and Engineering VIII*, Online Only, Spain, Sep. 2021, p. 12. doi: 10.1117/12.2596888.
[24] S. Zhang *et al.*, ‘Purification of Te75Ga10Ge15 glass for far infrared transmitting optics for space application’, *Opt. Mater.*, vol. 32, no. 9, pp. 1055–1059, Jul. 2010, doi: 10.1016/j.optmat.2010.02.030.